JOURNAL OF MATERIALS SCIENCE 20 (1985) 3353 – 3364

Fatigue behaviour of aligned short carbon-fibre reinforced polyimide and polyethersulphone composites

K. FRIEDRICH
Technical University Hamburg-Harburg, 2100 Hamburg 90, West Germany

K. SCHULTE
Deutsche Forschungs- und Versuchsanstalt, für Luft- und Raumfahrt, 5000 Köln 90, West Germany

G. HORSTENKAMP
Ruhr-University Bochum, 4630 Bochum, West Germany

T. W. CHOU
University of Delaware, Newark, Delaware 19716, USA

Fibre reinforced plastics, with 50 to 55 vol% of aligned short carbon fibres of approximately 3 mm in length, have good mechanical properties and advantages in deformability during the manufacturing process of structural components. The mechanical properties and damage mechanisms of this kind of composite have not been investigated deeply in the past. In the present paper results of an examination programme on laminates with various stacking sequences and two thermoplastic matrix systems (polyimide and polyethersulphone) are given. It will be shown that composites reinforced with aligned discontinuous carbon fibres can be an alternative material to continuous-fibre reinforced composites when considering their static and fatigue properties.

1. Introduction

Polymers reinforced with aligned short carbon fibres have become more and more interesting as materials for structural components, as they can be designed in complicated shapes with simultaneous satisfactory mechanical properties. A high alignment of the fibres yields an improvement in strength and stiffness of the composites in the fibre direction, so that the anisotropy of the properties of these materials is enhanced. This means that at the same time a reduction in the mechanical properties perpendicular to the fibre direction takes place. However, using the laminate technique which has been applied successfully in the design of materials with continuous fibres, prepegs of aligned short fibres can also be layered at different angles and be combined with each other in an autoclave process. In this way material design can be performed under the consideration of the loading conditions expected. Thus calculation methods known from laminate theory are also applicable to short-fibre reinforced plastics.

Although the mechanical behaviour is rather well understood and can also be described mathematically [1], the damage and failure mechanisms during a special type of loading are not well investigated. Only Moore [2] reports the experimental determination of the fatigue behaviour of short-fibre reinforced laminates.

It is the objective of the present paper (being a part of a more comprehensive study [3]) to investigate the mechanical behaviour of short carbon-fibre reinforced plastics, the resulting

0022–2461/85 $03.00 + .12

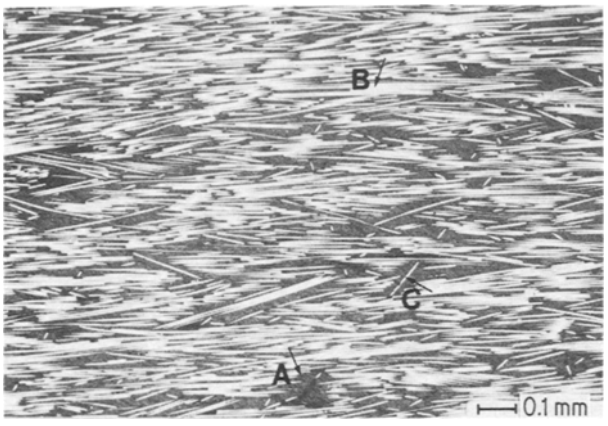

Figure 1 Polished cross-section of a PES $[0]_8$ laminate parallel to the fibre direction, showing resin-enriched regions (A), fibres of high degree of orientation aligned within separated fibre bundles (B), and individual misoriented fibres (C).

properties, and the damage and the failure mechanisms under static as well as fatigue loadings.

2. Experimental details

The experiments were carried out with aligned short carbon-fibre reinforced thermoplastics. Graphile XA–S (Courtaulds) had a fibre length of 3 mm; Polyimide (PI) Type H 795 E (Technochemie) and polyethersulphone (PES) from ICI were used as matrix systems. Fibre alignment was achieved by the vacuum drum filter technique [4], and the production of the laminates was performed in the central laboratory of MBB Co, in Ottobrunn/Munich. The individual plaques had a fibre volume fraction between 50 and 55%.

Laminates with the following stacking sequences were investigated: (a) unidirectional laminates $[0]_8$ and $[90]_8$; (b) multidirectional laminates $[0, 90, 0, 90]_s$ and $[0, \pm 45, 0]_s$. Additional measurements were carried out with the neat matrix materials.

Using flat tensile bars (composites: 200 mm × 25 mm, thickness 1.6 mm; resins; 150 mm × 10 mm, thickness 3.4 mm) fatigue experiments were carried out under tension–tension loading with a stress ratio of $R = \sigma_u/\sigma_o = 0.1$ and a frequency of $f = 10$ Hz (σ_o = upper stress level and σ_u = lower stress level per load cycle).

The additional use of strain gauges mounted on the specimens allowed one to register continuously changes in the stiffness of the material. Before starting the fatigue experiments, fracture strength and elongation at break as well as modulus and Poisson's ratio were determined in simple tensile tests with specimens of the same geometry at room temperature and a strain rate of 1 mm min^{-1}.

The characterization of the damage development by interruption of the fatigue tests after certain numbers of cycles, as well as the final analysis of the failure and breakdown mechanisms, were performed by a special X-ray technique, a replica method, and intensive optical microscopy and scanning electron microscopy (SEM). The different characterization techniques are described in detail in a previous paper [5].

3. Results and discussion

3.1. Microstructure of materials investigated

The alignment of short carbon fibres by applying the vacuum drum filter technique yields a very high degree of fibre orientation. This is illustrated by the polished cross-section taken parallel to the fibre direction of a PES $[0]_8$ laminate in Fig. 1. Although fibre alignment takes place in the form of separated fibre bundles, it can be observed that locally individual fibres exhibit a high deviation from the main fibre direction. There also exist resin-enhanced regions at the ends of fibre bundles as well as in the vicinity of misoriented individual fibres. During the preparation procedure of the laminates, void formation as a result of insufficient impregnating of the prepregs with matrix resin could not be avoided completely; in particular the PES laminates possessed a relatively high void density.

The PI and PES matrix materials chosen exhibit a very good thermal stability up to 200° C. This,

Figure 2 X-ray micrograph of a PI $[0, 90, 0, 90]_s$ specimen containing longitudinal microcracks (arrow) already in the non-loaded condition.

however, results in the fact that the processing temperature of these materials is higher than 200° C. As a consequence of the different thermal expansion coefficients, positive for the matrices and moderately negative to neutral for the fibres, a localized formation of microcracks along the 0° fibres, especially pronounced for the $[0, 90, 0, 90]_s$ laminates and to a lower amount in the $[0, \pm 45, 0]_s$ laminates, could be observed. In Fig. 2 these types of longitudinally arranged microcracks in a PI $[0, 90, 0, 90]_s$ laminate are made visible by the X-ray transmission technique used. In order to obtain a high resolution of the cracks, the specimens were treated with a contrast liquid (zinc iodide) which can penetrate into the cracks and leads to a high absorption contrast during the X-ray illumination.

3.2. Results of tensile tests

Table I represents the mechanical data (elastic modulus E, tensile strength σ_B, strain at break ε_B, Poisson's ratio ν) of the different resin materials and the corresponding laminates as obtained in the static tensile test. The neat PES resin possesses higher strain at break ε_B and a higher ultimate strength σ_B as compared to the polyimide. The same relationships are also measured for the $[90]_8$ laminates. The moderately lower elastic modulus of the polyethersulphone matrix material leads in the $[90]_8$ laminates also to lower values of stiffness. This means that the mechanical properties of a $[90]_8$ laminate are predominantly determined by the property profile of the matrix material used.

In the $[0]_8$, $[0, 90, 0, 90]_s$, $[0, \pm 45, 0]_s$ laminates, however, the static properties are mainly influenced by the fibres. This becomes especially clear from the fact that between the particular laminates with a different matrix system no significant difference in the elastic modulus exists. In the $[0, 90, 0, 90]_s$ and $[0, \pm 45, 0]_s$ laminates with a polyimide matrix higher values of ultimate strength as well as strain at break were achieved, as compared to those with a PES matix. Here it is assumed that the higher content of voids in the PES laminates has a negative influence, whereas in the $[0]_8$ laminates these voids are not yet effective.

3.3. Fatigue test results

Fig. 3a summarizes the results of fatigue tests with PI laminates. The highest stress level to achieve failure after, for example, 10^6 load cycles is necessary for the $[0]_8$ laminate (a factor of about two higher than the failure stresses for the $[0, \pm 45, 0]_s$ and $[0, 90, 0, 90]_s$ laminates, and

TABLE I Mechanical properties of materials, as measured in a tensile test

Material	PI matrix				PES matrix			
	E (GPa)	σ_B (MPa)	ε_B (%)	ν	E (GPa)	σ_B (MPa)	ε_B (%)	ν
resin	3.8	26	0.71	0.41	3	68	3.7	0.49
$[90]_8$	7.9	20	0.25	0.04	7.2	46	0.69	0.036
$[0]_8$	91	910	0.99	0.34	90	1000	1.09	0.42
$[0, 90, 0, 90]_s$	45	530	1.2	0.03	43	490	1.14	0.024
$[0, \pm 45, 0]_s$	50	600	1.21	0.61	51	600	1.18	0.68

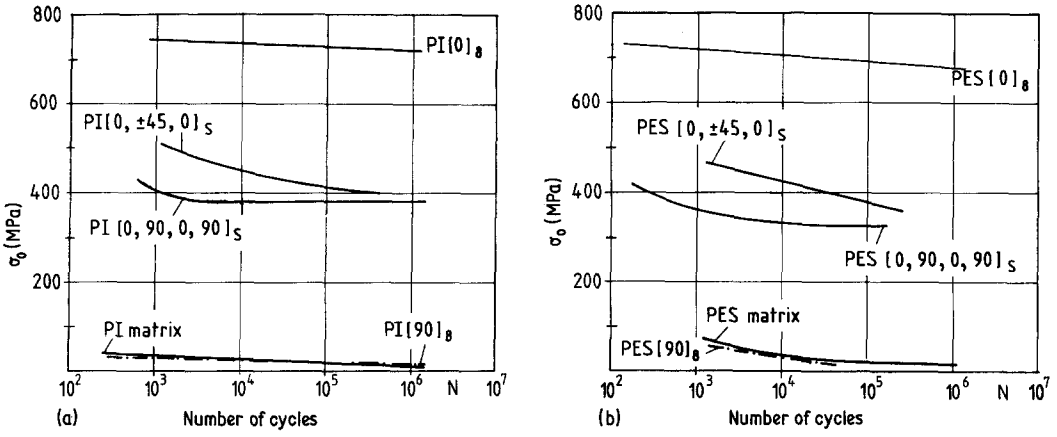

Figure 3 (a) Variation of upper stress level for failure with number of cycles to failure, for various PI laminates and for the neat resin material. (b) The corresponding curves for PES laminates and PES resin.

more than 20-fold higher than the values of the neat resin and the $[90]_8$ laminate). The slope of the ultimate failure curves for the different composites differs in the following way:

(a) For the $[0]_8$ laminate, the upper stress level necessary for failure in the range between 10^3 to 10^6 load cycles decreases linearly and only slightly, i.e. in a very narrow range between 750 and 720 MPa.

(b) A continuous and steeper reduction of the upper stress level is observed for the $[0, \pm 45, 0]_s$ laminate down to a value of 390 MPa if an endurance limit of 10^6 load cycles is considered.

(c) At a slightly lower load level as compared to the $[0, \pm 45, 0]_s$ laminates, the $[0, 90, 0, 90]_s$ laminates show a clear reduction of the upper stress limit in the range of low cycle fatigue (up to 10^4 cycles). In the region above $N = 10^4$ cycles, however, these curves tend to decrease only very slightly, as for the $[0]_8$ laminates.

(d) The neat polyimide resin as well as the $[90]_8$ laminate show a permanent reduction of the upper failure limit at the same, very low stress level.

The PES laminates (Fig. 3b) exhibit, in principle, the same tendencies as described for the PI laminates. The particular load levels are, however, slightly lower than those measured for the polyimide composites. This is assumed again to be a result of the existence of internal defects in the unloaded specimens. The matrix-dominated $[90]_8$ PES laminate reaches at higher load amplitudes (low cycle fatigue range) a longer endurance limit than the comparable PI material. This tendency changes, however, in the range of low-amplitude fatigue. Also this is an indication that possible defects such as voids in a PES laminate reduce its fatigue resistance. A comparison of the neat resin materials shows that PES is superior to PI in the range of low cycle fatigue (as in the static tensile test), whereas the long-term properties of both materials are quite similar.

A measure of the damage development in a laminate during fatigue loading is the change in stiffness during the load history [5, 6]. The variation in stiffness is determined by measurements of the secant elastic modulus. A decrease in the secant elastic modulus could be found for PI as well as PES laminates. As an example, Fig. 4a illustrates the reduction in stiffness of a PI $[0, 90, 0, 90]_s$ laminate, and Fig. 4b shows how the normalized secant modulus of a PI $[0, \pm 45, 0]_s$ laminate decreases with increasing percentage of the endurance limit of the composite material. As already observed for continuous-fibre reinforced laminates [7], the reduction in stiffness of the short-fibre reinforced laminates occurs in three steps. These are indicated in Figs. 4a and b as Regions 1, 2 and 3. Special mechanisms of damage development, which take place during the three different steps, will be discussed later. It should be mentioned that for the neat matrix materials, as well as for the $[0]_8$ and $[90]_8$ laminates, such a reduction of stiffness during fatigue loading was not observed.

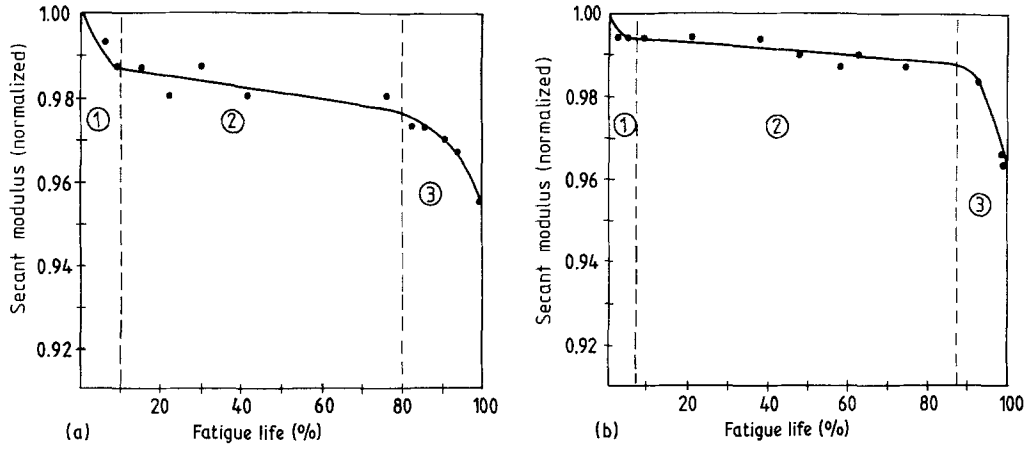

Figure 4 Normalized reduction of the secant elastic modulus as a function of the percentage of the endurance limit: (a) for PI $[0, 90, 0, 90]_s$ laminate; 2.5×10^4 cycles, $\sigma_0 = 370$ MPa; (b) for PI $[0, \pm 45, 0]_s$ laminate, 1.7×10^5 cycles, $\sigma_0 = 420$ MPa.

3.4. Analysis of damage development and failure mechanisms

3.4.1. Failure of $[0]_8$ *laminates*

The absence of a reduction in stiffness of the $[0]_8$ laminates during fatigue loading leads to the conclusion that spontaneous local failure, and not an overall damage development, finally caused complete fracture of the material. Sites of local failure could be detected by SEM analysis of the fracture surfaces. It turns out that these sites are directly related to the particular microstructure described in Section 3.1. Fracture mainly follows resin-enriched regions for which only a very insufficient reinforcement exists. The SEM micrograph in Fig. 5a gives a typical example for a resin-rich region at the end of a fibre bundle through which fracture development occurred. At these locations fibre pull-out can also be observed. It is indicated by individual stubs of fibres as well as circular holes in the matrix (Fig. 5b). Furthermore it can be recognized that poorly aligned fibres, partly oriented nearly perpendicularly to the 0° direction, are preferred sites of material breakdown. In the neighbourhood of non-oriented fibres, fibre fracture can also occur. In summary, all the possible mechanisms which dominate the fracture of $[0]_8$ laminates are schematically

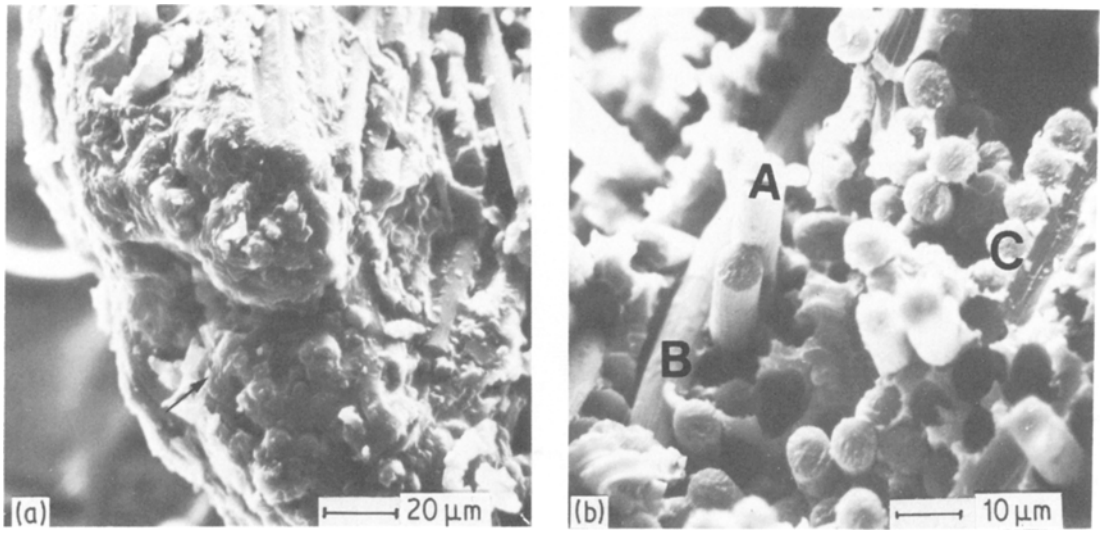

Figure 5 SEM fracture surface analysis of fatigued PI $[0]_8$ specimens: (a) resin-enriched region at the end of a fibre bundle (arrow); (b) fibre pull-out (A), poorly aligned fibres (B), and fibre fracture (C).

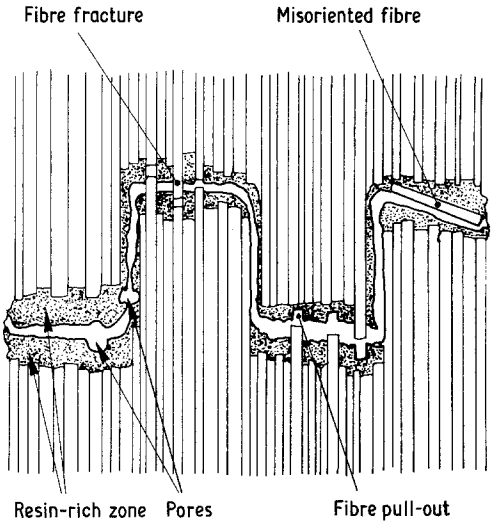

Figure 6 Schematic representation of the fracture paths and the individual fracture mechanisms in a $[0]_8$ composite.

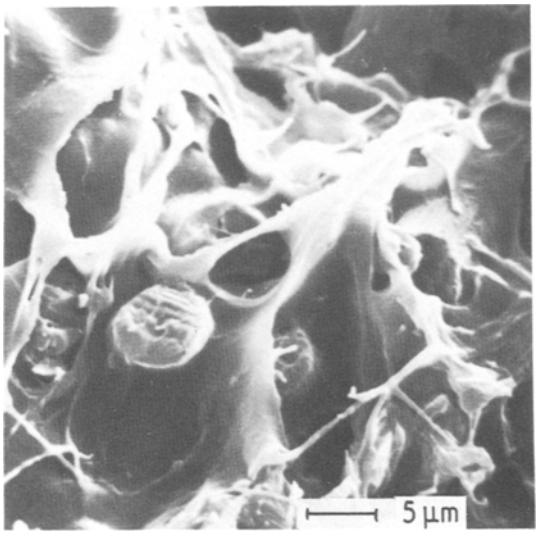

Figure 7 SEM fracture surface analysis of a PES $[0]_8$ fatigue sample, showing high plastic deformation of the matrix material in the fracture surface.

represented in Fig. 6. Voids, resin-enriched regions and individual fibres being only poorly aligned initiate the fracture, and are characteristic for the fracture surface morphology of unidirectional short-fibre reinforced composites.

The slight reduction in the fatigue strength of the $[0]_8$ laminates (compare Figs. 3a and b) has also been observed for unidirectional continuous-fibre reinforced composites [8]. However, no special defect structures can be detected by the X-ray technique. Also, the stiffness measurements did not show any reduction in the elastic modulus. As a consequence, these methods are not sensitive enough to detect any damage development in this material during fatigue loading. Fracture occurs relatively spontaneously, and equals roughly a typical fracture under static loading conditions. Therefore, the model of the fatigue fracture path given in Fig. 6 can also be used for the description of failure in statically loaded specimens.

The basic failure mechanisms are equal in PI and PES laminates; there exists, however, a difference in the degree of matrix deformation, which is higher for the PES $[0]_8$ laminates as a result of the higher strain at failure of the PES matrix (Fig. 7).

3.4.2. Failure of $[90]_8$ laminates

As already indicated in Table I, the static strength of the $[90]_8$ laminates is lower than those of the corresponding resin matrices. This is mainly due to locally enhanced stress concentrations introduced by the fibres in the surrounding resin matrix. Fig. 8 illustrates schematically how damage development in this kind of composite takes place. When such a material is loaded, regions with high as well as low fibre concentration have to be strained by the same amount. As a consequence of the higher modulus of the fibres (even perpendicular to the fibre direction) as compared to the matrix, in regions of high fibre content the matrix polymer is deformed much more than in adjacent resin-enriched regions in order to achieve strain equilibrium. Thus the deformation capacity of the matrix material is reached first in the regions of highest fibre content, so that the onset of fracture will take place there. In this way, the high ductility as well as strength of the PES relative to

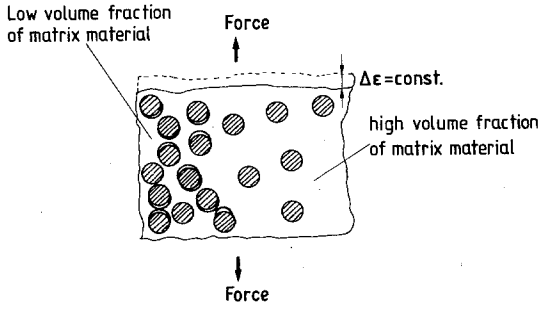

Figure 8 Schematic model of damage development in a 90° laminate in two region of different fibre–matrix distribution.

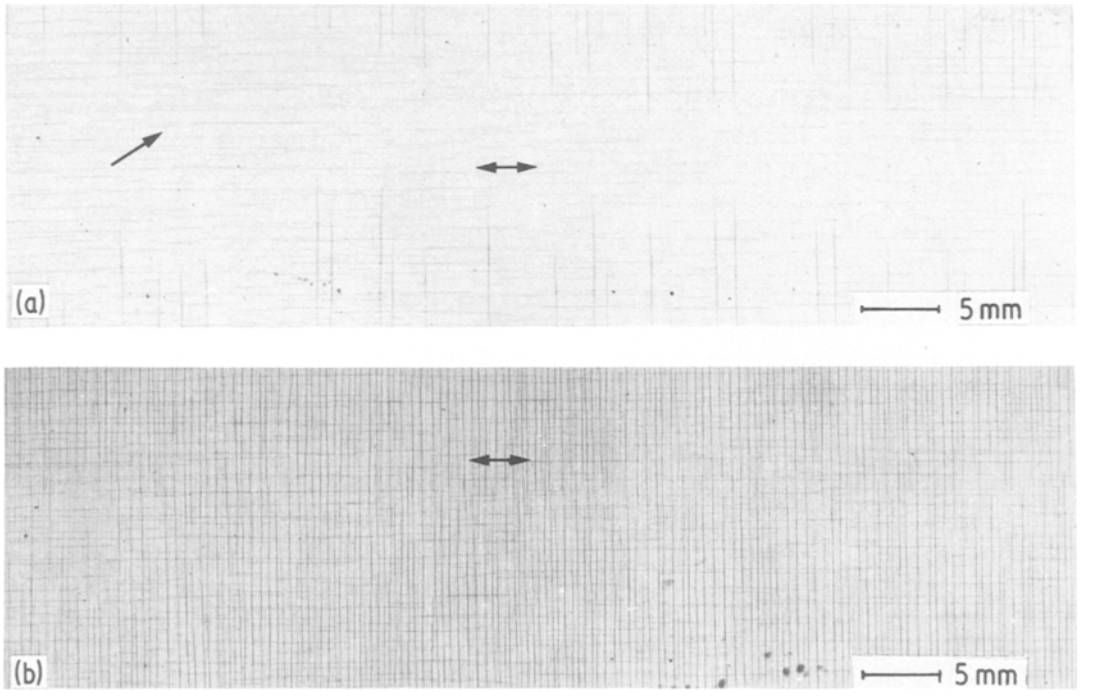

Figure 9 X-ray micrographs of a PI $[0, 90, 0, 90]_s$ tensile specimen. (a) Formation of transverse cracks at specimen edges and to a lower amount at individual longitudinal microcracks in the interior (arrow). The particular stress level at this damage state was $\sigma = 135$ MPa (double arrow = stress direction). (b) An example of the condition when the microcrack network is completed (CDS = characteristic damage state). This was reached at a stress level of $\sigma = 400$ MPa.

the PI resin is also reflected in the strength and strain of the corresponding $[90]_8$ composites.

3.4.3. Failure of $[0, 90, 0, 90]_s$ laminates

Failure behaviour of these kinds of composite under static loading is very similar to that observed for laminates with continuous-fibre reinforcement. Even at relatively low loads the formation of single transverse cracks starting from the specimen edges can be observed (Fig. 9a). The number of cracks increases with increasing load until an equilibrium stage is reached. At the same time, initially formed cracks have grown in length and finally cross the whole width of the specimen (Fig. 9b). This kind of equilibrium stage is known in the literature [7, 9] as the characteristic damage state (CDS).

Longitudinal cracks, which can already exist in PI $[0, 90, 0, 90]_s$ laminates prior to loading (see Fig. 2) are only limited to the surface layers. For the internal 0° layers, these longitudinal cracks could not be documented. It is assumed that there is not a direct influence of these longitudinal cracks on the strength of the material, especially because they do not grow during static loading. Nevertheless it could be shown that longitudinal cracks are able to initiate transverse cracks. The arrows on the X-ray micrograph given in Fig. 9a indicate those transverse cracks, which have formed at longitudinal cracks.

Under static load the onset of specimen fracture occurs at the moment of failure of the 0° layers. Damage development and failure mechanisms are in this case the same as already described for the unidirected $[0]_8$ laminates.

For PES composites of this type, damage development under static loading conditions seems to be similar. An exact X-ray analysis was not, however, possible as PES reacts very sensitively to the contrast liquid used.

Under fatigue loading there was found to be a reduction in the secant modulus of both the PI as well as the PES laminates (see Fig. 4a). This reduction in modulus took place in three phases, each of which was combined with a characteristic state of damage development. In Region 1 at the very beginning of the endurance limit transverse cracks are formed, which increase in number as well as length after a short number of cycles until an equilibrium stage the (CDS) for this type of

laminate is reached (Fig. 10a). These and the previous observations lead to the conclusion that the CDS is independent of the kind of loading (static tensile or fatigue loading), but depends strongly on the structure of the laminate and its individual components [7, 9, 10]. The influence of the CDS on the reduction of the secant modulus has been experimentally as well as analytically described in [11]. It is important to note here that during an early stage of fatigue loading the same mechanisms of damage development as are known from continuous-fibre reinforced plastics can occur also in short-fibre reinforced composite laminates.

Region 2 is primarily characterized by the progress of existing cracks and only to a small amount by the initiation of new cracks (Fig. 10b). The formation and growth of delaminations was not observed, which explains why in this region only a relatively small reduction in the secant modulus was detectable.

In Region 3 a failure mechanism is effective, which is typical for short-fibre reinforced laminates. Starting from the specimen edges longitudinal cracks are formed, which propagate at an angle of about 2° to the load direction in the 0° layers until the specimen ends are reached (Fig. 10c). A real explanation for this particular angle of crack direction does not exist at present; however, it is obvious that one reason for this angle is based on the alignment of the short fibres in bundles of about 75 μm in diameter and a length similar to the fibre length of 3 mm. It can be assumed that the cracks must usually follow these bundles (which in turn are not perfectly oriented) until they reach the bundle ends. Here, they can take the more favourable direction perpendicular to the applied load, i.e. through the resin-enriched regions. But this process is stopped soon by the interface of the next bundle, along which the crack is now forced to propagate. In fact, such a propogation mode results in an angle of crack direction which is very close to 2°.

A model for this propagation mode which was also found for an epoxy resin matrix reinforced with the same type of short fibres was first established by Helm [12]. At the edges of these longitudinal cracks further cracks are initiated at a later stage. These cracks as well as their time sequence are represented in Fig. 10d. The wedge-like fracture tips which are generated by this kind of crack progress finally delaminate the 90° layers adhering next to them, so that they are no longer capable of bearing any loads. Especially for this case a reduction of the load-carrying cross-sections of the external 0° layer by 10% results in an increase of load by about 2.6% in the residual 0° layers. This finally leads in a relatively short time to a complete failure of the specimen investigated.

The initiation of these longitudinal cracks at the specimen edges and the crack edges, respectively, is especially favoured by (a) resin enriched regions (Fig. 11a); (b) poorly aligned fibres (Fig. 11b); (c) voids (Fig. 11c); and (d) ends of fibre bundles (Fig. 11d). Schematically, the damage development in the specimen and the simultaneous reduction in the secant modulus is illustrated finally in Fig. 12.

3.4.4. *Failure of* $[0, \pm 45, 0]_s$ *laminates*

Fig. 13 represents an X-ray micrograph of a PI $[0, \pm 45, 0]_s$ specimen. Also in this type of specimen cracks are initiated under load at the edges of the specimen. Propagation occurs along the 45° fibres. The distance between these cracks becomes closer with increasing number of cycles until also for this specimen type the CDS is reached. There exists, however, a difference from the $[0, 90, 0, 90]_s$ laminates in the sense that in the present case these cracks do not propagate through the whole cross-section but grow only a few millimetres into the specimen.

The reduction in the secant elastic modulus during fatigue loading is the same as already observed for $[0, 90, 0, 90]_s$ laminates. Also the damage mechanisms in Regions 1 and 2 are very similar except for the difference in length between the transverse cracks and the 45° cracks. In Region 3, which is again associated with a strong reduction in the secant elastic modulus, the formation of longitudinal cracks is followed by an additional propagation of the 45° cracks. The latter process occurs, however, stepwise up to the edge of the longitudinal cracks right in front of the 45° cracks (Fig. 14).

For multidirectional laminates with a PES matrix, in principle, the same failure mechanisms occurred. But these were often accompanied by the formation and growth of delaminations which were then the dominant failure mechanisms, causing fracture of the specimen before other types of cracks completely developed. It

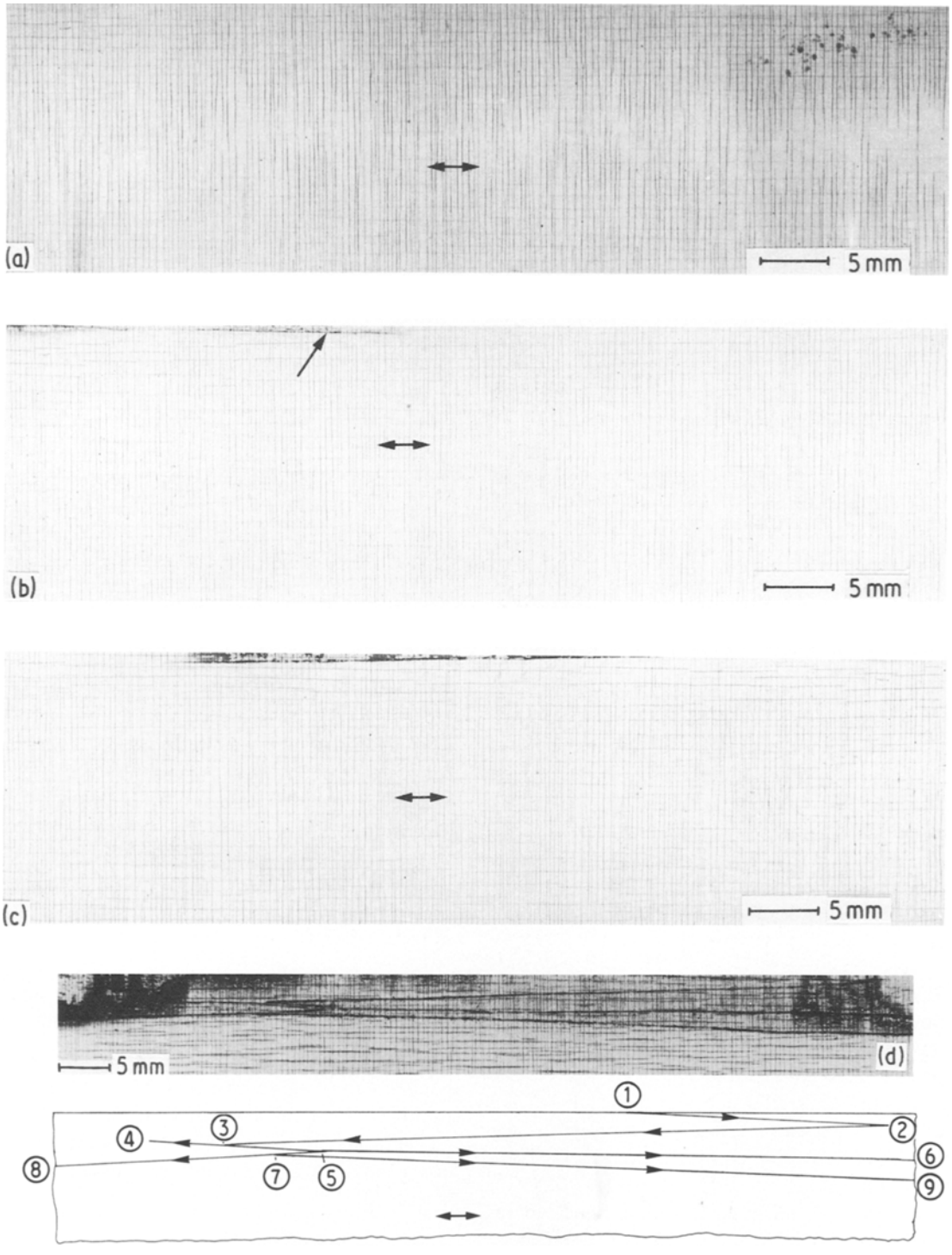

Figure 10 X-ray micrographs of a PI $[0, 90, 0, 90]_s$ specimen fatigued at an upper stress level of $\sigma_0 = 372$ MPa: (a) transverse crack pattern after 1000 load cycles; (b) onset of longitudinal crack growth in the outer 0° layers starting from specimen edges (arrow); (c) further growth of these longitudinal cracks and beginning of delamination between the cracked 0° layer and the adjacent 90° layer (darker regions at the upper edge); (d) time sequence of the formation and growth of longitudinal cracks, characterizing a condition just prior to final fracture of the material: 1 Crack initiation at the specimen edge, 2 change in crack direction, 3, 5, 7, new sites of crack initiation at edges of longitudinal cracks, 4, 6, 8, 9 crack tips running into specimen ends (double arrow = stress direction).

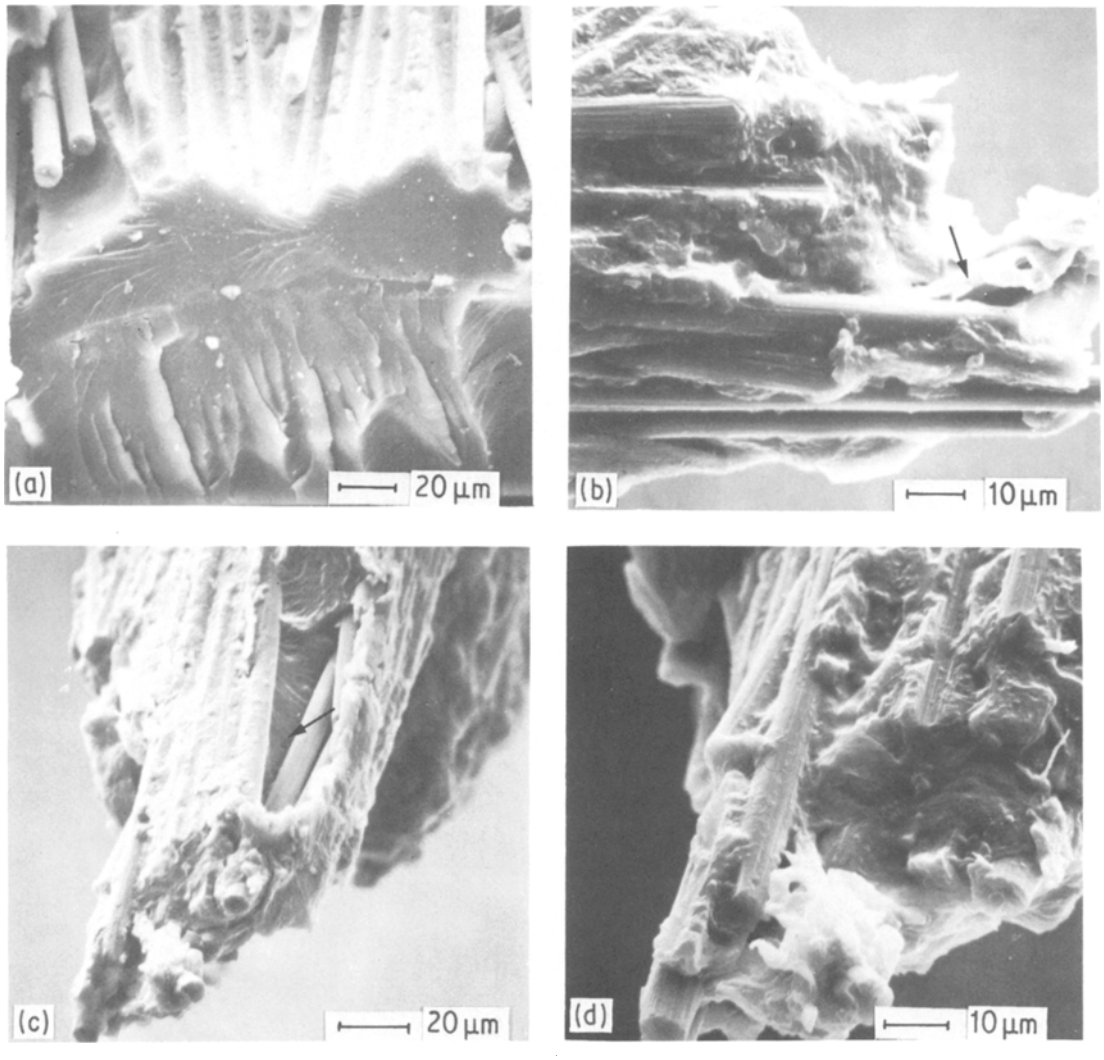

Figure 11 Scanning electron micrographs characterizing typical sites of longitudinal crack initiation in the 0° layers of PI fatigue specimens: (a) resin-enriched region; (b) poorly aligned individual fibres (arrow); (c) pores (arrow) in the vicinity of a wedge-like fractured piece formed by the initiation of a new longitudinal crack on the edge of another one, which before ran in the opposite direction (see Point 3 of Fig. 10d); (d) resin-enriched region at the end of a fibre bundle.

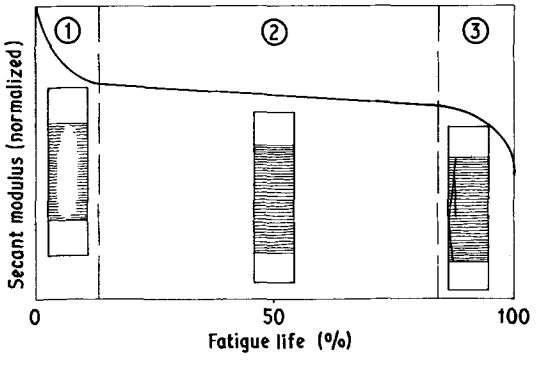

Figure 12 Schematic representation of damage development and simultaneous reduction in secant modulus of $[0, 90, 0, 90]_s$ laminates during fatigue.

seems that the formation of delaminations is not independent of aggressive environments like, for example, the contrast liquid used for X-ray micrography. But it can also be possible that a humid environment favours the delamination process [3].

4. Conclusions

Polymeric materials reinforced with aligned short carbon fibres can still possess relatively good mechanical properties which come close to their composite counterparts reinforced with continuous carbon fibres.

The failure mechanisms are nearly similar to

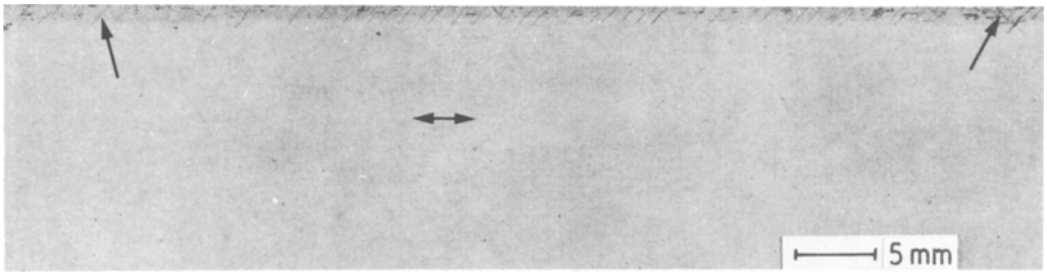

Figure 13 X-ray micrograph of a PI $[0, \pm 45, 0]_s$ tensile specimens at $\sigma = 520\,\text{MPa}$. Crack initiation (arrows) at the specimen edges under an angle $\pm 45°$ can be observed (double arrow = stress direction).

those in continuous-fibre reinforced laminates, which mainly means that during the course of a static but also a fatigue loading a dense network of internal cracks has to be established before fracture of the material takes place. Only in the case of the $[0]_8$ laminates were these crack patterns not observed as expected.

Fibre fracture is initiated by the growth of longitudinal cracks in the 0° layers. These cracks started at the specimen edges under an angle of about 2° so that propagation occurred in a direction towards the specimen ends. If new longitudinal cracks are initiated at points along the edges of previous longitudinal cracks a zig zag pattern is developed. Between the specimen edges and these longitudinal cracks delamination takes place so that the 0° layers are reduced in their load-carrying capacity. Favourable spots of crack initiation are inhomogenities in the material such as resin-enriched regions, misoriented individual fibres, and voids.

Acknowledgements

The authors would like to thank Dipl.- Ing. H. Richter, MBB Zentrallabor, Ottobrunn/ München, West Germany for preparation of the materials. The work was carried out at the Institute für Werkstoffe, DFVLR Köln, West Germany. K. Friedrich highly appreciates travel support by the Alexander von Humboldt Foundation. This paper was presented at the International Symposium "Composites: Materials and Engineering", Newark, USA, September, 1984.

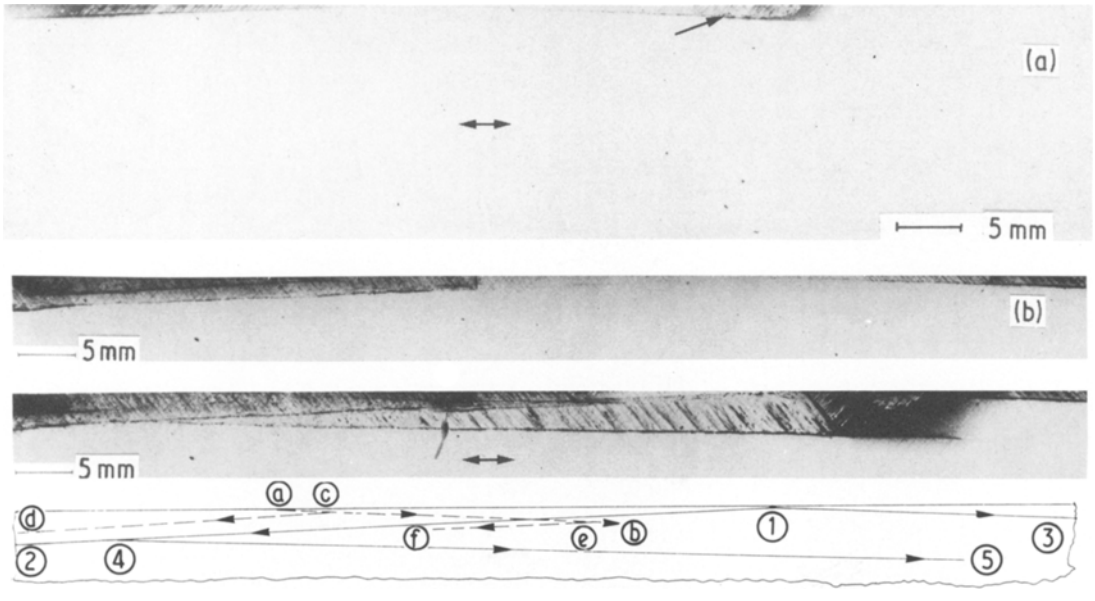

Figure 14 X-ray micrograph of a $[0, \pm 45, 0]_s$ specimen fatigued at an upper stress level of $\sigma_0 = 387\,\text{MPa}$: (a) represents the onset of longitudinal crack growth at the specimen edges (arrow); (b) gives an idea of the condition of the specimen just prior to final fracture, after the stepwise development of a longitudinal zig-zag crack pattern in both surface layers of the specimen (1 to 5 crack progress on upper and a to f on lower specimen side).

References

1. T. W. CHOU and A. KELLY, *Ann. Rev. Mater. Sci.* **10** (1980) 229.
2. B. B. MOORE, Proceedings of 3rd Risø International Symposium on Fatigue and Creep in Composite Materials, Roskilde, Denmark, September 1982 (Risø National Laboratory, Roskilde, Denmark) pp. 244–57.
3. K. SCHULTE, G. HORSTENKAMP and K. FRIEDRICH, "Mechanical Properties of Aligned Short Carbon Fibre Reinforced PES and PI Laminates", European Space Agency, Technical Translation No. ESA-TT-898, February 1985, Translation of DFVLR-FB-84-24, (Wissenschaftliches Berichtswesen der DFVLR, Köln, West-Germany, 1984) pp. 1–100.
4. H. RICHTER, "Verarbeiten und Anwenden kohlenstoffaserverstärkter Kunststoffe" (VDI-Gesellschaft Kunststofftechnik, Düsseldorf, West Germany, 1981) pp. 243–57.
5. K. SCHULTE, E. G. HENNEKE II and J. C. DUKE, Proceedings of DGM conference "Verbundwerkstoffe — Stoffverbunde", Konstanz, West Germany, May 1984, (Deutsche Gesellschaft für Metallkunde, Bad Homburg, West-Germany, 1984) to be published.
6. H. T. HAHN and R. W. KIM, *J. Compos. Mater.* **10** (1976) 156.
7. K. SCHULTE, K. L. REIFSNIDER and W. W. STINCHCOMB, Proceedings of 18 AVK-Jahrestagung, Freudenstadt, West Germany, October, 1982, (Arbeitsgemeinschaft Verstärkte Kunststoffe, Frankfurt, West-Germany, 1982) pp. 29.1–29.8.
8. M. J. OWEN, "Fracture and Fatigue", edited by L. J. Brontman (Academic, New York, 1974) pp. 242–56.
9. K. L. REIFSNIDER, Proceedings of the 14th Annual Meeting, Society of Engineering Science, Lehigh University, Bethlehem, USA (The American Society for Mechanical Engineers, 1977) pp. 343–384.
10. J. E. MASTERS and K. L. REIFSNIDER, ASTM STP 775 (American Society for Testing and Materials, Philadelphia, 1982) pp. 40–62.
11. A. L. HINGHSMITH and K. L. REIFSNIDER, *ibid.*, pp. 103–40.
12. H. HELM, "Bruch- und Schwingfestigkeitsverhalten von uniaxialen Kohlenstoff-Kurzfaser/Epoxidharz-Verbunden", internal report, Ruhr University Bochum–DFVLR (Wissenschaftliches Berichtswesen der DFVLR, Köln, West-Germany, 1981) pp. 1–49.

Received 11 October
and accepted 6 November 1984